A Spectroscopic Analysis of Phase Separation Behavior of Polyurethane in Restricted Geometry: Chain Rigidity Effects

Hun-Jan Tao, Curtis W. Meuse,† Xiaozhen Yang, William J. MacKnight, and Shaw L. Hsu*

Polymer Science and Engineering Department and Materials Research Science and Engineering Center, University of Massachusetts, Amherst, Massachusetts 01003

Received February 28, 1994; Revised Manuscript Received August 26, 1994®

ABSTRACT: Phase separation behavior associated with ultrathin films of model polyurethanes has been studied by reflectance infrared spectroscopy. Our data clearly demonstrate that the phase separation behavior and the domain size of polyurethanes in the ultrathin film region differ significantly from its bulk state. The kinetics measured are considerably slower than the bulk state. In addition, the degree of phase separation is also highly dependent on film thickness. The phase separation obeys an *Avrami* type rate process. Using a *Monte Carlo* simulation method to fix the location and orientation of the nucleating points, the phase separation behavior can be modeled. The relatively slow rate of phase separation, the ultimate degree of phase separation, and the observed high value of chain orientation on the substrate are consequences of having a polyurethane with semirigid hard segments.

Introduction

Segmented polyurethane elastomers are alternating block copolymers consisting of flexible soft segments and more rigid hard segments. A variety of techniques have revealed a phase-separated morphology, with hard segments mainly residing in hard segment rich domains.[1,2] This relatively pure phase coexists with one containing mainly soft segments with some hard segments dispersed in it.[3] Formation of hydrogen bonds, crystallization of hard segments, chain folding, excluded volume effect, and kinetics arguments have all been proposed as possible explanations for this phase separation behavior.[1-6] In our previous study, we proposed that the excluded volume effect associated with the stiffness of the hard segment is an important factor for phase separation for the [methylene bis(phenyl isocyanate)] (MDI)-based system.[6] The phase diagrams calculated for the system containing MDI extended by diacetylenes as hard segment mixed with poly(propylene glycol) (PPG) as the soft segment are consistent with experimental results.[7]

The basic assumption in our past studies is that if the excluded volume effect of the hard segments is important, the hard segments will phase separate into disk-like domains with nematic-like structure due to the strong lateral interactions between them.[6,7] It is most convenient to characterize the phase separation behavior by following the relative intensity of the two components generally seen in the C=O stretching ($\sim$1700 cm^{-1}) region. The higher frequency component is assigned to the carbonyl stretching free from hydrogen bonding. The lower frequency component is characteristic of hydrogen-bonded carbonyls in phase-separated domains. The phase separation kinetics can be determined from the change in the relative intensity of the two components as a function of time.[8] In some cases, segmental orientation needs to be taken into account.[8] Our previous spectroscopic analyses have shown that a spinodal decomposition mechanism does not fit the data well.[9] Instead a model forming disk-like domain can be used to explain the kinetics observed. An *Avrami-like* analysis yielded a coefficient $\sim$2.[9]

In a follow-up study, we used the thermal reflectance technique to monitor the relative intensity of the two carbonyl stretchings in the 1700 cm^{-1} region for polyurethanes on various substrates. Our data suggested a high degree of segmental orientation on the substrates.[8] After taking this structural anisotropy into account, we have been able to demonstrate that the ultimate degree of phase separation is also highly dependent on film thickness. In this current study, we have carried out kinetics experiments similar to the ones we conducted in the past. We found, most surprisingly, that the phase separation kinetics measured in extremely thin polyurethane films, on the order of 10s or 100s of angstroms thick, are quite different, i.e., much slower, as compared to the ones measured for the bulk state.[9] The factors governing the structure formation in a restricted geometry, e.g., an ultrathin film on a substrate, are unknown, and the transition from the bulk to the thin film structure is unclear. Intuitively, the degree of phase separation and the orientation of the phase-separated domains are expected to be dependent on the length of the hard segments. Theory predicts that the orientation caused by the surface would only affect the first three or four layers from the interface between the air and the polymer.[10-13]

It is our hypothesis that the slow phase separation kinetics and the lowering of the degree of phase separation in extremely thin films are directly related to the constraints of the air-solid interface.[14-16] Intuitively, semirigid hard segments simply lack the translational freedom to form hard segment rich domains in extremely thin films as compared to the bulk state. In this current study, based on the spectroscopic data obtained, we have formulated and solved the mass transport equation to form hard segment rich domains with the boundary conditions defined by the air-solid interfaces. Using the model developed, we were able to analyze this aspect as well. There is little doubt that chain rigidity influences strongly the formation of phase-separated structure in thin films. Our results are reported here.

Experimental Section

The polyurethane (B2 polymer) used in these experiments has been described previously.[17] The monodisperse hard segment consists of three MDI units extended by two butanediol linkages. The soft segment is a 2000 molecular weight poly(propylene glycol) (PPG). The gold surfaces for infrared external reflection

* To whom correspondence should be addressed.
† Department of Chemistry. Current address: National Institute of Health, Betheda, MD.
® Abstract published in *Advance ACS Abstracts*, October 15, 1994.

0024-9297/94/2227-7146$04.50/0

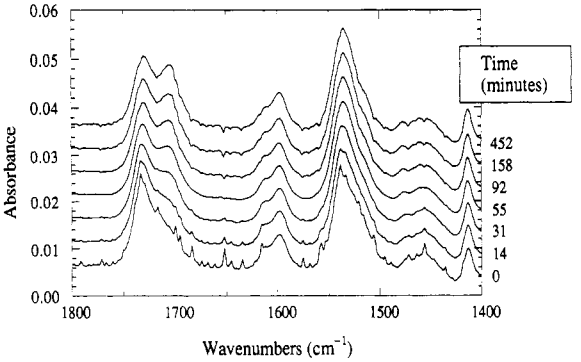

Figure 1. Reflection infrared spectra for the phase separation process of a 16 nm B2 polymer film on gold at 23 °C.

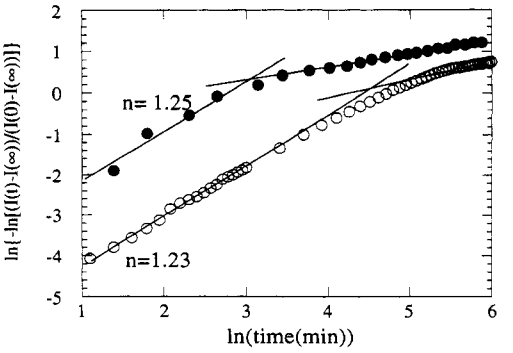

Figure 2. Isothermal phase separation kinetics for a 16 nm thick film on gold at 23 °C: experimental results (●) and simulated results (○) using a disk model.

experiments are 200 nm thick 99.999% gold-coated microscope slides prepared by the Brysen Optical Co. of Safety Harbor, FL. The 16 nm B2 polymer films are formed by casting one drop of 2.5 mg/mL polyurethane in tetrahydrofuran (THF) solution directly onto the surface of glycerine. The glycerin is then heated to ~60 °C, and the film is transferred by placing the gold surface face down onto the film. In this fashion it is possible to attach the polyurethane to the gold substrate. Since glycerin is soluble in water, any residual glycerin in the sample is removed by rinsing the sample in water heated to ~60 °C. Other film thicknesses are produced by spin casting (using a Headway Research Inc. spin coater at 3000 rpm for 30 s) directly onto the gold surfaces from 0.01 to 0.5% (weight per volume) solutions in THF. The continuity and film thicknesses were checked by contact angle and ellipsometry methods as described previously.[8]

The infrared spectra are obtained with a Nicolet 60SXB spectrometer equipped with a narrow-band MCT detector using an external reflection cell purchased from Specac Ltd. of Milford, CT. All spectra were collected at 2 cm^{-1} resolution. The external reflection cell holds the sample in a horizontal position that allows it to be easily modified to incorporate a heating block beneath the sample in order to obtain spectra at variable temperatures. The temperature of the heating block could be controlled to within 1 °C using an Omega programmable temperature controller and a copper-constantin thermocouple sensor. In order to conduct the phase separation experiment, the molten sample can be cooled to a desired temperature in the sampling chamber of this reflection cell. We have built another heating unit immediately adjacent to the reflectance cell to melt the sample. It possible to transfer the sample from the molten state to the reflectance unit set at the desired phase separation temperature without opening the sample chamber. The temperatures can be controlled sufficiently well, so that data collection can be started within 10 s after the sample is transferred into the reflectance cell.

In order to obtain spectra as a funcition of time, a program was written that initially collects 10 sets of 64 scans and later collects 109 sets of 512 scans. We have used an incident infrared radiation with polarization parallel to the scattering plane defined by the incident and reflected rays. The incident angle has been set to 86°. Once the kinetic experiment is completed, all 119 files are Fourier transformed and ratioed against a constant background. Changes in the infrared spectra for a 16 nm B2 polymer films are shown in Figure 1. The kinetics data for the much thicker film, >2 μm, of B2 polymer have been published earlier.[9]

Results and Discussion

I. Experimental Results. In all of our polyurethane studies, a two-phase approximation is used. Phase separation kinetics have been characterized by infrared spectroscopy using two different carbonyl bands in the amide I region representing the two phases. The higher frequency band at 1730 cm^{-1} is assignable to hard segments that are surrounded by soft segments (free from hydrogen bonding), and the lower frequency band at 1700 cm^{-1} is associated with hard segments hydrogen bonded to each other. The relative intensity of these two bands is usually indicative of the degree of phase separation. If the sample is heated to above its phase mixing point and then quenched to a temperature below the phase-mixing temperature to begin the phase separation process, isothermal phase separation kinetics can be determined by analyzing the amide I band changes as a function of temperature and time. This type of kinetics experiment has been carried out in previous studies to study the phase separation behavior in thick films (considered to be bulk-like).[9] In that case, because the signal available is sufficiently strong, infrared spectroscopy was easily carried out using the standard transmission mode. In cases when the samples are thin, on the order of 10s of nanometers, the most convenient method is to use the reflectance technique.[8] Figure 1 is an example of the isothermal phase separation spectra for a 16 nm B2 polymer film. Unlike the transmission experiment of an isotropic film, however, the degree of phase separation of an ultrathin film cannot be simply determined by the relative intensity of the two amide I bands obtained with the reflectance technique, since preferential orientation usually is present.[8] The boundary conditions associated with reflections from a dielectric film on a metallic substrate are such that only vibrations with transition moments in the scattering plane (p polarization) can be observed. Therefore, the apparent relative intensity of the bands seen in the amide I region can be associated either with differences in the degree of phase separation or in the orientation of molecules on the surface. For anisotropic ultrathin films studied by external reflection, however, the different relative intensities observed as compared to the isotropic film represent the degree of phase separation as well as the orientation of the urethane groups on the substrate. A procedure for separating effects arising in phase separation from those related to segmented orientation follows.[8]

After correcting for spectroscopic anomalies using procedures described earlier,[8] an Avrami-type analysis has been applied to characterize the phase separation kinetics of polyurethanes as described previously.[9] In this model, the volume fraction of phase separated domains, $X(t)$, is expressed as

$$X(t) = 1 - \exp(-kt^n) \quad (1)$$

where k is the rate constant and n is described as the Avrami exponent. The value of the exponent has been used to suggest different types of phase transformation mechanisms.[18]

Data presented in Figure 2 for a 16 nm film show an initial slope of 1.25 changing to ~0.6 at later stages. The change in the slope can be interpreted as due to the decrease in concentration of hard segments in the isotropic phase.[9] Growth of the phase-separated domains can only be continued when other hard segments diffuse to the

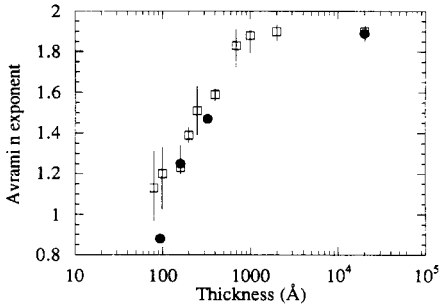

Figure 3. Comparison of kinetics exponents as a function of film thickness for B2 polymer at 23 °C: experimental results (●) and simulated results (□) based on a disk model.

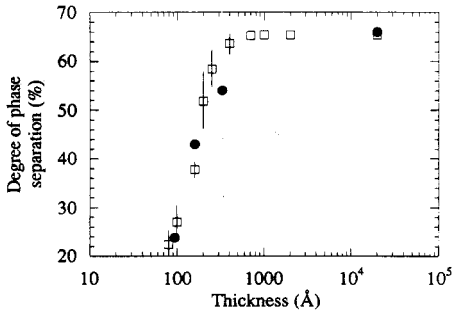

Figure 4. Comparison of ultimate degree of phase separations as a function of film thickness for B2 polymer at 23 °C: experimental results (●) and simulated results (□) based on a disk model.

domain surface. This exponent is considerably smaller than the one we found for the bulk state. In that case, the value is in the range of 1.8–2.0 in the initial stage changing over to 0.6 at later stages. In addition, in this study we found that the value of the first exponent strongly depends on film thickness. It decreases with decreasing film thickness. In addition, we found the ultimate degree of phase separation achievable, i.e., the degree of phase separation at extremely long time, also decreases with film thickness. These results are summarized in Figures 3 and 4.

II. Model Used To Analyze Phase Separation Kinetics. In our study we hypothesize that geometric effects associated with chain stiffness and strong lateral intermolecular interactions should be considered. If the hard segment is fairly flexible, the hard segment rich domains are expected to form isotropic structures such as spheres. In contrast, if the chains are rigid and coupled with strong intermolecular interactions, then disk-like hard segment rich domains are favored to form as suggested earlier.[6] The type of domains formed will result in different kinetics. This is particularly so for phase separation in restricted geometry such as in air–solid interface. It is important to develop a model to explain in a quantitative fashion the kinetics as shown in Figures 2 and 3. In addition, the dramatic change in the degree of phase separation in ultrathin film region (Figure 4) also needs explanation. Lastly, the anisotropic property of the film formed is an extremely important factor and should be incorporated in the model.

For analytical calculation, it is difficult to take into account the experimental data described above; therefore, a nucleation and growth process incorporating the Monte Carlo method is used for simulating the phase separation process. The simulation is off-lattice type and is assumed to proceed in a box with a lateral dimension of 1.5 μm and a variable thickness ranging from 8 nm to 2 μm. The hard segment is taken to be 5 nm in length based on our simulation studies. The domain growth is assumed to be

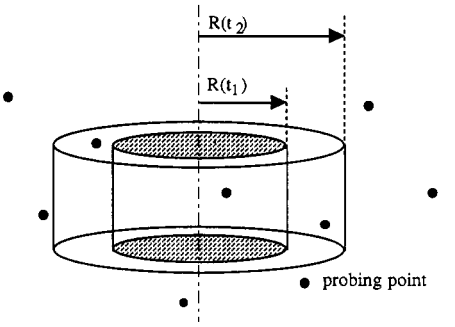

Figure 5. Schematic illustration of the domain growth at various time and the measurement of $X(t)$ by the probing points.

heterogeneous. The chain rigidity of the hard segment is taken into consideration so the disk-like model has been adapted for the growing entity. The location and orientations of *nuclei* are determined by the Monte Carlo method. Because these hard segments are assumed to be rigid, not all positions or orientations of the nuclei obtained by the Monte Carlo method are acceptable. Given the initial position and orientation of the nuclei at $t = 0$, i.e., the first segment, it is possible to monitor concentric cylindrical growth with the center axis being the orientation of the first segment. The sizes of the concentric cylinders at various time are determined by the growth rate constant, G, and the hard segment concentration in the isotropic phase. There are two parameters, G and the number of nuclei per unit volume, necessary for our analysis which are determined from the data obtained for the 2 μm and 16 nm thick films. Initial estimates for these two values are fitted to the two exponents measured for a 2 μm thick film. Then the best fit is used to calculate the exponents and the ultimate degree of phase separation for the 16 nm thick film at 20 °C. Iterative calculations were carried out until the two parameters fit the kinetics data for both the 2 μm and 16 nm films. The determined G value is 25 nm/min and the number of nuclei per unit volume is 1080 μm^{-3}.

The phase-separated domains are allowed to *grow* when an additional 10 000 probing points are placed randomly into the box. The volume fraction of phase-separated domains, $X(t)$, is determined by the fraction of probing points which are located within the domains at a particular cylinder (Figure 5). To test whether a probing point falls inside growing entities in order to measure $X(t)$, the following algorithms have been used for the disk-like domain. If the distance from a probing point to the center line of a disk is smaller than the disk radius, and this probing point falls between the two surfaces of the disk, then the probing point is accepted. It is immediately evident that the phase separation rate and Avrami exponent will decrease significantly if the growing domains are on the same order of size as the film thickness because many points are excluded from further consideration as a function of time. This is shown schematically in Figure 6. This factor is extremely important in thin films but negligible for a thick film. In this fashion we have satisfied the experimental observation that high anisotropy has been observed for these films particularly in extremely thin samples.

Our experimental data whether for bulk or in thin films have always suggested a changing kinetics as a function of time. The phase separation slows significantly at long time. In all cases involving linear growth, the rate only depends on the concentration profile of hard segments in the isotropic phase. This changing kinetics can be seen

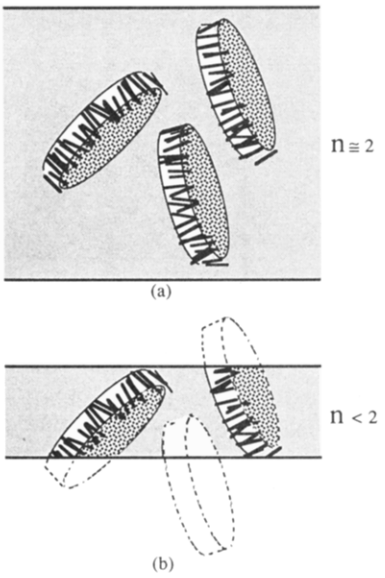

Figure 6. Schematic illustration of film thickness effect on phase separation kinetics: (a) thick film; (b) thin film which has smaller n and lower degree of phase separation.

as follows, assuming R_g is the growth rate of hard domains

$$R_g(t) = \frac{dV}{dt} = \frac{A(t)\Delta R(t)}{\Delta t} \tag{2}$$

where $A(t)$ is the active surface area at time t and ΔR is the hard domain size increment within a small time interval Δt. The driving force for hard segments diffusing toward the hard segment rich domains is the hard segment concentration gradient near the domain surface, which can be expressed as

$$R_g = -k\nabla C|_{surface} \tag{3}$$

The hard segment concentration profile is shown in Figure 7. C_0 is the hard segment equilibrium concentration near the hard domain surface while C_1 and C_2 are the hard segment concentrations in the isotropic phase. Lengths AB and CD in Figure 7 can be defined as the diffusion boundary layer thicknesses at times t_1 and t_2, which increase as the isotropic concentration decreases. To simplify the calculation, the diffusion boundary layer thicknesses AB and CD are assumed to be constant (Figure 7b). This assumption is a good one for at least the early stage of phase separation. The phase separation rate can then be expressed as

$$R_g(t) \cong G[C(t) - C_0]A(t) \tag{4}$$

where $C(t)$ is the hard segment concentration in the isotropic phase and G is the rate constant that is assumed to be independent of time. From eqs 2 and 4, we have

$$\Delta R(t) = GF_c\Delta t \tag{5}$$

F_c is a concentration factor defined as

$$F_c(t) = C(t) - C_0 \tag{6}$$

Be definition, $C(t)$ is the mass of hard segments in the isotropic phase divided by the volume of the isotropic phase at time t. Then

$$C(t) = \frac{C_T - X(t)}{1 - X(t)} \tag{7}$$

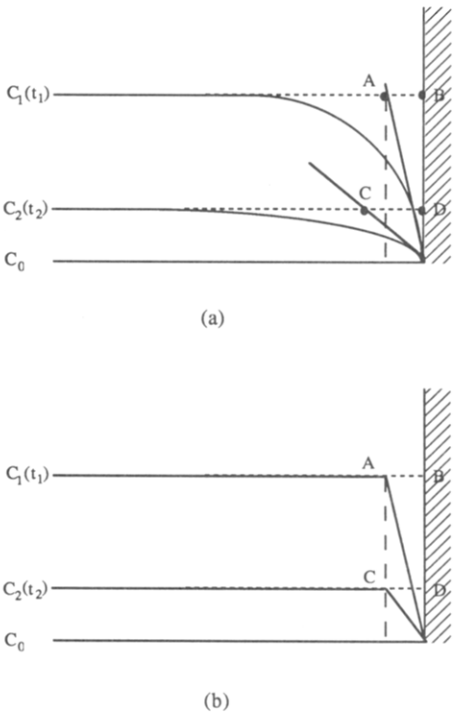

Figure 7. Schematic illustration of the hard segment concentration profile from the hard domain surface to the isotropic phase: (a) actual profile; (b) linear concentration profile in the diffusion boundary layer as an approximation used in this simulation.

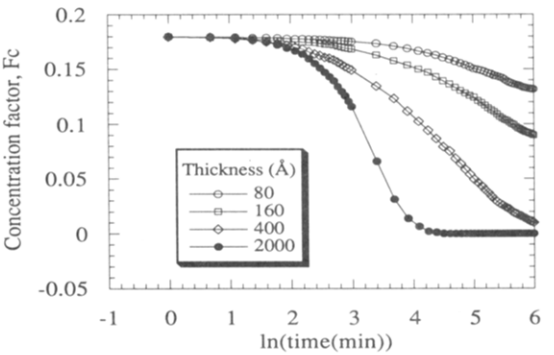

Figure 8. Changes in the concentration factor F_c for different film thicknesses simulated by disk model.

where C_T is the overall hard segment concentration. Combining eqs 6 and 7, the concentration factor can be expressed as

$$F_c(t) = \frac{C_T - X(t)}{1 - X(t)} - C_0 \tag{8}$$

which can be determined by $X(t)$ if C_0 and C_T are known. As can be seen below, the dramatic decrease of $F_c(t)$ at the later stages of phase separation may cause the changing slope as seen in Figures 8 and 9. C_T of B2 polyurethane is 0.32. C_0 is estimated to be 0.14 taken as the hard segment concentration in isotropic phase of a 2 μm B2 polymer film by infrared spectroscopy. This estimation is based on the assumption that hard domains consist of pure hard segments.[6,19] The exact C_0 value may be slightly different from the ones used in our analysis. Our predictions, however, will not be affected. The impingement effect has been considered, but the hindrance of the disk lateral growth blocked by other disk surfaces is ignored due to the low C_T value. The blocking effect will further decrease the exponent n and the ultimate degree of phase separation.

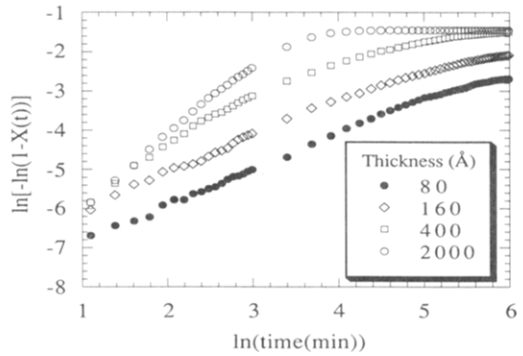

Figure 9. Simulated Avrami plots for several film thicknesses for disk model.

Finally, specific interactions or adsorption of polyurethanes to the supporting surface are neglected.

III. Comparison of Simulation to Experiment. The simulated kinetics curves of the entire series of films with varying thicknesses are shown in Figure 9. All the important features observed in our experiment, i.e., changing kinetics and the degree of phase separation as a function of film thickness, have been reproduced with accuracy. The calculated exponents are summarized in Figure 3. The error bars are associated with different random number sequences. These simulated results show that the exponent, n, starts to deviate from the one measured for the bulk state at a film thickness of ~10 times the hard segment length (~50 nm) due the restriction effect of the air–solid interface. The final degree of phase separation is determined by the plateau $X(t)$ value and is plotted in Figure 4. Decrease in the final degree of phase separation is well-reproduced by our simulation. We have also clearly shown that having an air–solid interface starts to affect the degree of phase separation if the film thickness is smaller than 10 times the hard segment length. The voids within the film as shown in Figure 6b cannot be filled by the growing domains and will result in a lower degree of phase separation and Avrami exponent compared with the thick film case (Figure 6a). Obviously, the decrease in the degree of phase separation for thin polyurethane films is kinetically controlled and is a consequence of chain rigidity.

The principal difference between simulation and experiment is that slope change occurs at later time in the calculations than in the experiment (Figure 2). This deviation is attributed to the approximation of a constant diffusion boundary layer thickness. Using this approximation will result in a higher diffusion rate in the later stages than the actual case. To obtain better agreement between simulation and experiment, a more exact concentration profile describing the boundary layer thickness change needs to be included. The initial exponent or the final degree of phase separation calculated will not be affected by this approximation.

IV. Analysis of Structural Anisotropy. Because of chain rigidity, the growth of the hard segment rich domain is restricted to the lateral direction due to the strong cohesive interactions between segments. When domains reach to the interface, either air–solid or solid–substrate, no more growth can occur. In thinner films there are fewer possible orientations (virtually all the segments need to be oriented parallel to the surface) for hard segments to be located in the film. Based on the spectroscopic data obtained, we found a very high degree of chain orientation for thin polyurethane films, if the film thickness is of the same order as the hard segment length. Our infrared external reflection experimental data have shown the hard

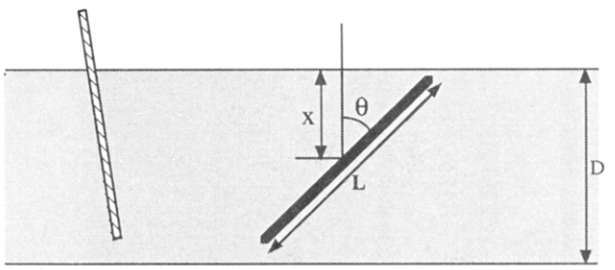

Figure 10. Schematic illustration of the preferential orientation effect of hard segment in an ultrathin film; Dashed rod: forbidden orientation. Solid rod: allowed orientation with geometric variables used in the text.

segments of B2 polymer begin to exhibit preferential orientation for films thinner than 32.8 nm, which is ~6 times the hard segment length. The orientation observed is strongly dependent on film thickness, although the exact values of orientation for extremely thin films have been difficult to determine because of insufficient signal to noise ratios obtained for those samples. We have rationalized the existence of significant segmental orientation as shown below.

Assuming L is the rigid rod length and D is the film thickness (Figure 10), if the center of the rod is located within a distance x of the surface which is smaller than $L/2$, then there exists a minimum θ for this rod to be confined within the film with an angle

$$\theta_{\min} = \cos^{-1}\left(\frac{x}{L/2}\right) \tag{9}$$

With the rod center in this location, the averaged $\cos^2\theta$ with all allowed orientations is

$$\begin{aligned}\langle\cos^2\theta\rangle &= \frac{\int_{\theta_{\min}}^{\pi/2} 2\pi(L/2)^2 \sin\theta\cos^2\theta\,d\theta}{\int_{\theta_{\min}}^{\pi/2} 2\pi(L/2)^2 \sin\theta\,d\theta} \\ &= {}^1/_3\cos^2\theta_{\min} \\ &= {}^4/_3\left(\frac{x}{L}\right)^2 \end{aligned} \tag{10}$$

For a film with thickness smaller than the rod length, with rod centers randomly distributed inside the film, we have

$$\begin{aligned}\langle\cos^2\theta\rangle &= \frac{\int_0^{D/2} {}^4/_3\left(\frac{x}{L}\right)^2 dx}{D/2} \\ &= \left(\frac{D}{3L}\right)^2 \qquad (L \geq D) \end{aligned} \tag{11}$$

With eq 11, we can calculate the orientation distribution function most appropriate for rigid chains, f, as

$$\begin{aligned} f &= \frac{3\langle\cos^2\theta\rangle - 1}{2} \\ &= \frac{{}^1/_3(D/L)^2 - 1}{2} \qquad (L \geq D) \end{aligned} \tag{12}$$

For a film thicker than the rod length, we have

$$\begin{aligned}\langle\cos^2\theta\rangle &= \frac{{}^1/_9 L + {}^1/_3(D-L)}{D} \\ &= {}^1/_3 - {}^2/_9\left(\frac{L}{D}\right) \qquad (D \geq L) \end{aligned} \tag{13}$$

which is based on the fact that $\langle\cos^2\theta\rangle$ is $^1/_9$ if D equals L (eq 11) and is $^1/_3$ for the isotropic case. Using eq 13, the

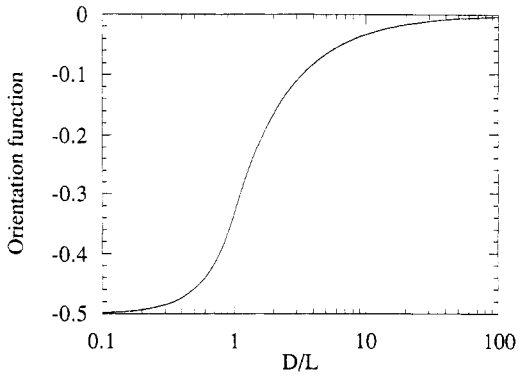

Figure 11. Calculated orientation function of rods confined within two surfaces. D is the film thickness and L is the rod length.

orientation function for a film thicker than the hard segment length is

$$f = {}^1/_3\left(\frac{L}{D}\right) \qquad (D \geq L) \tag{14}$$

Figure 11 clearly shows that for rigid rods confined within two surfaces the preferential orientation of hard segments is high when the film thickness is smaller than 10 times the rod length. This prediction is consistent with our experimental data and Monte Carlo simulation results. We can also *safely* define a "thick film", i.e., a film absent of effects from having constraints from surfaces or interfaces, as having a thickness much greater than $10L$. Direct comparison of the orientation functions derived from infrared spectra to the calculated ones is difficult, though, because the exact transition dipole moment direction of the carbonyl groups and the precise hard segment structures need to be determined. These two results, however, show quite consistent trends if we assume that the carbonyl transition dipole moment direction is approximately perpendicular to the chain axis.

Conclusions

The relatively slow rate of phase separation, the ultimate degree of phase separation, and the observed high value of chain orientations on the substrate are consequences of having a polyurethane with semirigid hard segments. Our reflectance infrared measurements have been used to analyze the phase-separated structures in thin films. The phase separation obeys an Avrami-type rate process. From this, the growth rate constant can be obtained. Then using a Monte Carlo simulation method to fix the location and orientation of the points, the process can be modeled using two parameters, the growth rate alluded to above and the number density of nuclei. We conclude that the hard segment rigidity is very important and it might be the dominating driving force for phase separation for the B2 polymer. For longer hard segments it may not be able to keep the whole chain from bending, but the chain rigidity should still dominate the phase separation process. Finally, this work clearly demonstrates that the phase separation behavior and the domain size of polyurethanes in the ultrathin film region differ significantly from its bulk state. Their differences in other physical properties are also expected.

Acknowledgment. This research has been supported by a grant from Army Research Office, Grant no. DAAL03-91-G-0127. In addition, a fellowship from Rohm & Haas to one of us (H.J.T.) is greatly appreciated.

References and Notes

(1) Petrovic, Z. S.; Ferguson, J. *J. Prog. Polym. Sci.* **1991**, *16*, 695.
(2) Hepburn, C. *Polyurethane elastomers*; Applied Sciences Publishers: London, 1982.
(3) Koberstein, J. T.; Leung, L. M. *Macromolecules* **1992**, *25*, 6205.
(4) Koberstein, J. T.; Stein, R. S. *J. Polym. Sci., Polym. Phys. Ed.* **1983**, *21*, 1439.
(5) Li, Y.; Ren, Z.; Zhao, M.; Yang, H.; Chu, B. *Macromolecules* **1993**, *26*, 612.
(6) Tao, H.-J.; Hsu, S. L.; MacKnight, W. J. *Polym. Prep. (Am. Chem. Soc., Div. Polym. Chem.)* **1992**, *33* (2), 575.
(7) Tao, H.-J.; MacKnight, W. J.; Hsu, S. L. *Macromolecules* **1994**, *27*, 1720.
(8) Meuse, C. W.; Yang, X.; Yang, D.; Hsu, S. L. *Macromolecules* **1992**, *25*, 925.
(9) Lee, H. S.; Wang, Y. K.; MacKnight, W. J.; Hsu, S. L. *Macromolecules* **1988**, *21*, 270.
(10) Helfand, E. *J. Chem. Phys.* **1975**, *63*, 2192.
(11) Yoon, D. Y.; Flory, P. J. *Macromolecules* **1988**, *17*, 868.
(12) Theodoro, D. N. *Macromolecules* **1988**, *21*, 1411.
(13) Theodoro, D. N. *Macromolecules* **1988**, *21*, 1422.
(14) Stein, R. S.; Powers, J. *J. Polym. Sci.* **1962**, *56*, S9.
(15) Escleine, J. M.; Monasse, B.; Wey, E.; Haudin, J. M. *Colloid Polym. Sci.* **1984**, *262*, 363.
(16) Billon, N.; Escleine, J. M.; Haudin, J. M. *Colloid Polym. Sci.* **1989**, *267*, 668.
(17) Christenson, C. P.; Harthcock, M. A.; Meadows, M. D.; Spell, H. L.; Howard, W. L.; Creswick, M. W.; Guerra, R. E.; Turner, R. B. *J. Polym. Sci., Polym. Phys. Ed.* **1986**, *24*, 1401.
(18) Wunderlich, B. *Macromolecular Physics*; Academic Press: New York, 1976; Vol. 2, Chapter 6.
(19) Kornfield, J. A.; Spiess, H. W.; Nefzger, H.; Eisenbach, C. D. *Macromolecules* **1991**, *24*, 4787.